

MURA Dataset: Towards Radiologist-Level Abnormality Detection in Musculoskeletal Radiographs

Pranav Rajpurkar^{*1} Jeremy Irvin^{*1} Aarti Bagul¹ Daisy Ding¹ Tony Duan¹
 Hershel Mehta¹ Brandon Yang¹ Kaylie Zhu¹ Dillon Laird¹ Robyn L. Ball²
 Curtis Langlotz³ Katie Shpanskaya³ Matthew P. Lungren³ Andrew Ng¹

Abstract

We introduce MURA, a large dataset of musculoskeletal radiographs containing 40,895 images from 14,982 studies, where each study is manually labeled by radiologists as either normal or abnormal. On this dataset, we train a 169-layer densely connected convolutional network to detect and localize abnormalities. Six board-certified radiologists provide additional labels for a test set of 209 studies, on which we compare model and radiologist performance. We find that our model achieves performance comparable to that of radiologists. On finger, hand, and wrist studies, our model’s F1 scores are slightly higher than those of radiologists, but not statistically significantly so; on elbow, forearm, humerus, and shoulder studies our model’s F1 scores are slightly lower than those of radiologists, but also not statistically significantly so, indicating that the dataset presents a good challenge problem for future research. The dataset is freely available at <https://stanfordmlgroup.github.io/projects/mura>.

1. Introduction

Large, high-quality datasets have played a critical role in driving progress of fields with deep learning methods (Deng et al., 2009). To this end, we introduce MURA, a large dataset of radiographs, containing 14,982 musculoskeletal studies of the upper extremity. Each study contains one or more views (images) and is manually

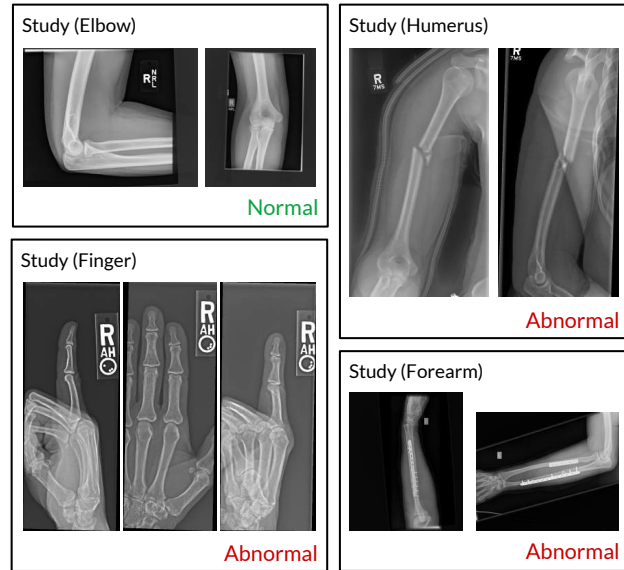


Figure 1. The MURA dataset contains 14,982 musculoskeletal studies of the upper extremity, where each study contains one or more views and is manually labeled by radiologists as either normal or abnormal. These examples show a normal elbow study (top left), an abnormal humerus study with a fracture (top right), an abnormal finger study with degenerative changes (bottom left), and an abnormal forearm study (bottom right) demonstrating operative plate and screw fixation of radial and ulnar fractures.

labeled by radiologists as either normal or abnormal.

The abnormality detection task, or in other words determining whether a radiographic study is normal or abnormal, is a critical radiological task: a study interpreted as normal rules out disease and can eliminate the need for patients to undergo further diagnostic procedures or interventions. Musculoskeletal conditions affect more than 1.7 billion people worldwide (BMU, 2017), and are the most common cause of severe, long-term pain and disability (Woolf & Pfleger, 2003), with 30 million emergency department visits an-

^{*}Equal contribution ¹Stanford University Department of Computer Science ²Stanford University Department of Medicine ³Stanford University Department of Radiology. Correspondence to: Pranav Rajpurkar <pranavsr@cs.stanford.edu>, Jeremy Irvin <jirvin16@cs.stanford.edu>.

Study	Normal	Abnormal	Total
Elbow	1,203	768	1,971
Finger	1,389	753	2,142
Forearm	677	380	1,057
Hand	1,613	602	2,215
Humerus	411	367	778
Shoulder	1,479	1,594	3,073
Wrist	2,295	1,451	3,746
Total	9,067	5,915	14,982

Table 1. MURA contains 9,067 normal and 5,915 abnormal musculoskeletal radiographic studies of the upper extremity including the shoulder, humerus, elbow, forearm, wrist, hand, and finger. MURA is one of the largest public radiographic image datasets.

nually and increasing. Our dataset, MURA, contains 9,067 normal and 5,915 abnormal musculoskeletal radiographic studies of the upper extremity including the shoulder, humerus, elbow, forearm, wrist, hand, and finger. MURA is one of the largest public radiographic image datasets.

On MURA, we develop a competitive abnormality detection model. The model takes as input one or more views for a study of an upper extremity. On each view, a 169-layer convolutional neural network predicts the probability of abnormality; the per-view probabilities are then averaged to output the probability of abnormality for the study.

To evaluate models robustly and to get a estimate of radiologist performance, we collected six additional labels from board-certified radiologists on a holdout test set of 209 studies. We compare the performance of our model and radiologists, and find that our model achieves performance comparable to that of radiologists. On finger, hand, and wrist studies, our model’s F1 scores are slightly higher than those of radiologists, but not statistically significantly so; on elbow, forearm, humerus, and shoulder studies our model’s F1 scores are slightly lower than those of radiologists, but also not statistically significantly so. We have made our dataset freely available to encourage advances in medical imaging models.

2. MURA

The MURA abnormality detection task is a binary classification task, where the input is an upper extremity radiograph study — with each study containing one or more views (images) — and the expected output is a binary label $y \in \{0, 1\}$ indicating whether

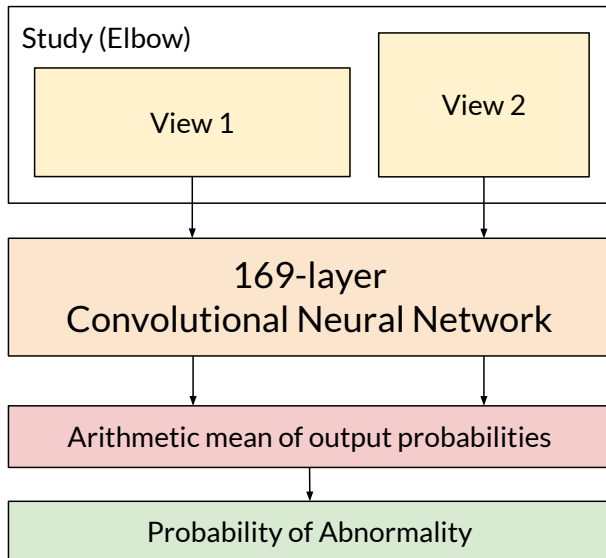


Figure 2. The model takes as input one or more views for a study. On each view, our 169-layer convolutional neural network predicts the probability of abnormality; the per-view probabilities are then averaged to output the probability of abnormality for the study.

the study is normal or abnormal respectively.

2.1. Data Collection

Our institutional review board approved study collected de-identified, HIPAA-compliant images from the Picture Archive and Communication System (PACS) of Stanford Hospital. We assembled a dataset of musculoskeletal radiographs consisting of 14,982 study from 12,251 patients, with a total of 40,895 multi-view radiographic images. Each belongs to one of seven standard upper extremity radiographic study types: elbow, finger, forearm, hand, humerus, shoulder, and wrist. Table 1 summarizes the distribution of normal and abnormal studies.

Each study was manually labeled as normal or abnormal by board-certified radiologists from the Stanford Hospital at the time of clinical radiographic interpretation in the diagnostic radiology environment between 2001 and 2012. The labeling was performed during interpretation on DICOM images presented on at least 3 megapixel PACS medical grade display with max luminance 400 cd/m^2 and min luminance 1 cd/m^2 with pixel size of 0.2 and native resolution of 1500 x 2000 pixels. The clinical images vary in resolution and in aspect ratios. We split the dataset into training (11,255 patients, 13,565 studies, 37,111 images), validation (788 patients, 1,208 studies, 3,225 images),

	Radiologists (95% CI)	Model (95% CI)
Study F1		
Elbow	0.858 (0.707, 0.959)	0.848 (0.691, 0.955)
Finger	0.781 (0.638, 0.871)	0.792 (0.588, 0.933)
Forearm	0.899 (0.804, 0.960)	0.814 (0.633, 0.942)
Hand	0.854 (0.676, 0.958)	0.858 (0.658, 0.978)
Humerus	0.895 (0.774, 0.976)	0.862 (0.709, 0.968)
Shoulder	0.925 (0.811, 0.989)	0.857 (0.667, 0.974)
Wrist	0.958 (0.908, 0.988)	0.968 (0.889, 1.000)
Aggregate F1	0.884 (0.853, 0.918)	0.857 (0.804, 0.905)

Table 2. We compare radiologists and our model on the F1 metric, which is the harmonic average of the precision and recall of the models, where precision (positive predictive value) is the fraction of abnormal studies among the studies predicted as abnormal, while recall (sensitivity) is the fraction of abnormal studies predicted as abnormal. The F1 score reaches its best value at 1 (perfect precision and recall) and worst at 0. Model performance is higher than radiologist performance on finger, hand, and wrist studies. Radiologist performance is higher on elbow, forearm, humerus, and shoulder studies.

and test (208 patients, 209 studies, 559 images) sets. There is no overlap in patients between any of the sets.

2.2. Test Set Collection

To evaluate models robustly and to get an estimate of radiologist performance, we collected additional labels from board-certified Stanford radiologists on the test set, consisting of 209 musculoskeletal studies. The radiologists individually reviewed and labeled each study in the test set as a DICOM file retrospectively as normal or abnormal in the clinical reading room environment using the clinical PACS system. The radiologists have 8.83 years of experience on average ranging from 2 to 25 years. The radiologists did not have access to any clinical information. Labels were entered into a standardized data entry program.

2.3. Abnormality Analysis

To investigate the types of abnormalities present in the dataset, we reviewed the radiologist reports to manually label 100 abnormal studies with the abnormality finding: 53 studies were labeled with fractures, 48 with hardware, 35 with degenerative joint diseases, and 29 with other miscellaneous abnormalities, including lesions and subluxations.

3. Model

The model takes as input one or more views for a study of an upper extremity. On each view, our 169-layer convolutional neural network predicts the probability of abnormality. We compute the overall probability of abnormality for the study by taking the arithmetic

mean of the abnormality probabilities output by the network for each image. The model makes the binary prediction of abnormal if the probability of abnormality for the study is greater than 0.5. Figure 2 illustrates the model’s prediction pipeline.

3.1. Network Architecture and Training

We use a 169-layer convolutional neural network to predict the probability of abnormality for each image in a study. The network uses a Dense Convolutional Network architecture – detailed in Huang et al. (2016) – which connects each layer to every other layer in a feed-forward fashion to make the optimization of deep networks tractable. We replace the final fully connected layer with one that has a single output, after which we apply a sigmoid nonlinearity.

For each image X of study type T in the training set, we optimize the weighted binary cross entropy loss

$$\begin{aligned} L(X, y) = & -w_{T,1} \cdot y \log p(Y = 1|X) \\ & -w_{T,0} \cdot (1 - y) \log p(Y = 0|X), \end{aligned}$$

where y is the label of the study, $p(Y = i|X)$ is the probability that the network assigns to the label i , $w_{T,1} = |N_T|/(|A_T| + |N_T|)$, and $w_{T,0} = |A_T|/(|A_T| + |N_T|)$ where $|A_T|$ and $|N_T|$ are the number of abnormal images and normal images of study type T in the training set respectively.

Before feeding images into the network, we normalize each image to have the same mean and standard deviation of images in the ImageNet training set. We then scale the variable-sized images to 224×224 . We

Dataset	Study Type	Label	Images
MURA	Musculoskeletal (Upper Extremity)	Abnormality	41,299
Pediatric Bone Age (AIMI)	Musculoskeletal (Hand)	Bone Age	14,236
0.E.1 (OAI)	Musculoskeletal (Knee)	K&L Grade	8,892
Digital Hand Atlas (Gertych et al., 2007)	Musculoskeletal (Left Hand)	Bone Age	1,390
ChestX-ray14 (Wang et al., 2017)	Chest	Multiple Pathologies	112,120
OpenI (Demner-Fushman et al., 2015)	Chest	Multiple Pathologies	7,470
MC (Jaeger et al., 2014)	Chest	Abnormality	138
Shenzhen (Jaeger et al., 2014)	Chest	Tuberculosis	662
JSRT (Shiraishi et al., 2000)	Chest	Pulmonary Nodule	247
DDSM (Heath et al., 2000)	Mammogram	Breast Cancer	10,239

Table 3. Overview of publicly available medical radiographic image datasets.

augment the data during training by applying random lateral inversions and rotations.

The weights of the network are initialized with weights from a model pretrained on ImageNet ([Deng et al., 2009](#)). The network is trained end-to-end using Adam with default parameters $\beta_1 = 0.9$ and $\beta_2 = 0.999$ ([Kingma & Ba, 2014](#)). We train the model using mini-batches of size 8. We use an initial learning rate of 0.0001 that is decayed by a factor of 10 each time the validation loss plateaus after an epoch, and pick the model with the lowest validation loss.

4. Results

4.1. Evaluation

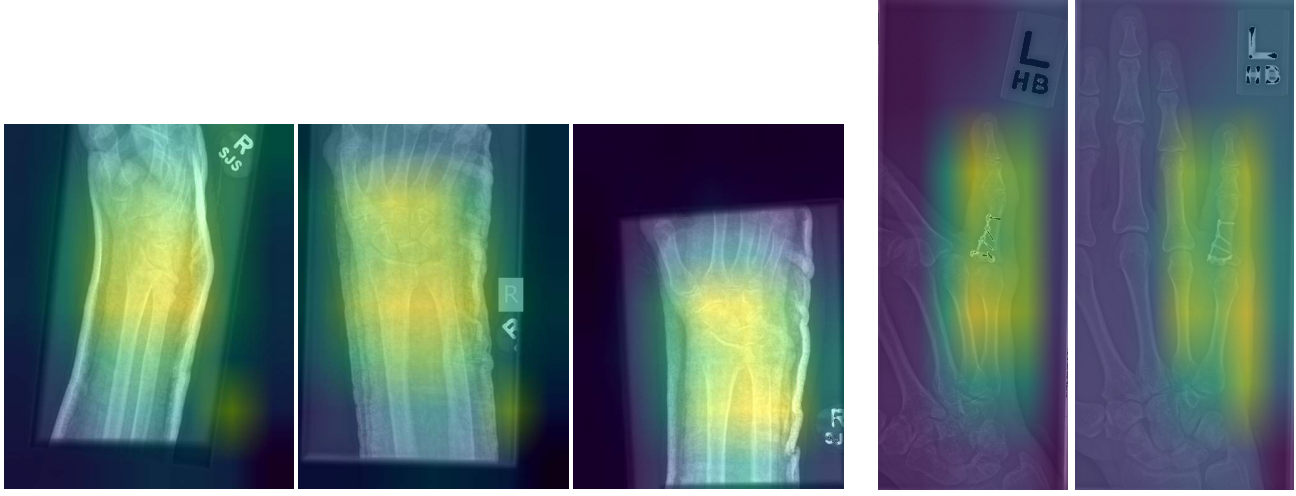
We evaluate models using the F1 metric. The F1 metric is the harmonic average of the precision and recall of the models, where precision (positive predictive value) is the fraction of abnormal studies among the studies predicted as abnormal, while recall (sensitivity) is the fraction of abnormal studies predicted as abnormal. The F1 score reaches its best value at 1 (perfect precision and recall) and worst at 0.

4.2. Radiologist vs. Model Performance

We assessed the performance of both radiologists and our model on the test set. Recall that for each study

in the test set, we have additional labels from 6 board-certified radiologists. To evaluate radiologists, we compute the F1 score of individual radiologist labels using the majority vote of the labels provided by the other 5 radiologists as ground truth. We similarly evaluate models, by computing the F1 score of the model predictions against each group of 5 radiologists, using the group’s majority vote as the ground truth. We report the mean of the resulting 6 F1 scores of the radiologists and the model. We used the bootstrap to construct 95% bootstrap confidence intervals (CIs), as follows: for each subtype (and in aggregate), we calculated the average F1 score for both the model and the radiologists on 10,000 bootstrap samples, sampled with replacement from the test set. We also calculated the difference between the average F1 score for the model and the average F1 score for the radiologists on the same bootstrap samples. We took the 2.5th and 97.5th percentiles of the F1 scores as the 95% bootstrap CI. If the 95% CI on the difference did not include zero, we concluded there was a significant difference between the F1 score of the model and the F1 score of the radiologists.

Table 2 summarizes the performance of both radiologists and the model on the different study types and in aggregate. The radiologists achieve their best performance on wrist studies with an F1 score of 0.958 (95% CI 0.908, 0.988) and their lowest performance on finger



(a) Three views of the right wrist in a patient with distal radius and ulna fractures after casting. The model predicts the probability of abnormality in each view to be greater than 99%, correctly predicting the study as abnormal.

(b) Two radiographic views of the finger in a patient with a prior fifth proximal phalynx fracture status post screw and plate fixation. The model predicts the probability of abnormality in both views to be greater than 99.9%, correctly predicting the study as abnormal.

Figure 3. Our model localizes abnormalities it identifies using Class Activation Maps, which highlight the areas of the radiograph that are most important for making the prediction of abnormality.

studies 0.781 (95% CI 0.638, 0.871). The model also achieves its best performance on wrist studies with an F1 score of 0.968 (95% CI 0.889, 1.000), and its lowest performance on finger studies 0.792 (95% CI 0.588, 0.933). Model performance is higher than radiologist performance on finger, hand, and wrist studies, and radiologist performance is higher on elbow, forearm, humerus, and shoulder studies. Overall, the radiologist performance at an F1 score of 0.884 (95% CI 0.853, 0.918) is higher than the model F1 score of 0.857 (95% CI 0.804, 0.905). However, all differences are within the confidence interval ranges, so the performance of the model is statistically indistinguishable from that of the radiologists.

5. Model Interpretation

We visualize the parts of the radiograph which contribute most to the model’s prediction of abnormality by using class activation mappings (CAMs) (Zhou et al., 2016). We input the radiograph X into the fully trained network to obtain the feature maps output by the final convolutional layer. To compute the CAM $M(X)$, we take a weighted average of the feature maps using the weights of the final fully connected layer. Denote the k th feature map output by the network on image X by $f_k(X)$ and the k th fully connected weight by w_k . Formally,

$$M(X) = \sum_k w_k f_k(X).$$

To highlight the salient features in the original radiograph which contribute the most to the network predictions, we upscale the CAM $M(X)$ to the dimensions of the image and overlay the image. We provide several examples of CAMs along with radiologist commentary in Figure 3.

6. Related Work

Large datasets have led to deep learning algorithms achieving or approaching human-level performance on tasks such as image recognition (Deng et al., 2009), speech recognition (Hannun et al., 2014), and question answering (Rajpurkar et al., 2016). Large medical datasets have led to expert-level performance on detection of diabetic retinopathy (Gulshan et al., 2016), skin cancer (Esteva et al., 2017), heart arrhythmias (Rajpurkar et al., 2017a), brain hemorrhage (Grewal et al., 2017), pneumonia (Rajpurkar et al., 2017b), and hip fractures (Gale et al., 2017).

There has been a growing effort to make repositories of medical radiographs openly available. Table 3 provides a summary of the publicly available datasets of medical radiographic images. Previous datasets are smaller

than MURA in size, with the exception of the recently released ChestX-ray14 (Wang et al., 2017), which contains 112,120 frontal-view chest radiographs with up to 14 thoracic pathology labels. However, their labels were not provided directly from a radiologist, but instead automatically generated from radiologists' text reports.

There are few openly available musculoskeletal radiograph databases. The Stanford Program for Artificial Intelligence in Medicine and Imaging hosts a dataset containing pediatric hand radiographs annotated with skeletal age (AIMI). The Digital Hand Atlas consists of left hand radiographs from children of various ages labeled with radiologist readings of bone age (Gertych et al., 2007). The OsteoArthritis Initiative hosts the O.E.1 dataset which contains knee radiographs labeled with the K&L grade of osteoarthritis (OAI). Each of these datasets contain less than 15,000 images.

7. Discussion

Abnormality detection in musculoskeletal radiographs has important clinical applications. First, an abnormality detection model could be utilized for worklist prioritization. In this scenario, the studies detected as abnormal could be moved ahead in the image interpretation workflow, allowing the sickest patients to receive diagnoses more quickly. Furthermore, the examinations identified as normal could be automatically assigned a preliminary reading of "normal"; this could mean (1) normal examinations can be properly triaged as lower priority on a worklist (2) more rapid results can be conveyed to the ordering provider (and patient) which would improve disposition in other areas of the healthcare system (i.e., discharged from the ED more quickly) (3) a radiology report template for the normal study can be served to the interpreting radiologist for more rapid review and approval.

Second, automated abnormality localization could help combat radiologist fatigue. Radiologists all over the world are reading an increasing number of cases with more images per case. Physician shortages exacerbate the problem, especially for radiologists in medically underserved areas (Nakajima et al., 2008). While physician fatigue is a common problem that affects all healthcare professionals, radiologists are particularly susceptible, and there is evidence that workloads are so demanding that fatigue may impact diagnostic accuracy. (Bhargavan & Sunshine, 2005; Lu et al., 2008; Berlin, 2000; Fitzgerald, 2001). A study examining radiologist fatigue in the interpretation of musculoskeletal radiographs found a statistically significant decrease in fracture detection at the end of the work

day compared to beginning of work day (Krupinski et al., 2010). Thus, a model which can perform automatic abnormality localization could highlight the portion of the image that is recognized as abnormal by the model, drawing the attention of the clinician. If effective, this could lead to more efficient interpretation of the imaging examination, reduce errors, and help standardize quality. More studies are necessary to evaluate the optimal integration of this model and other deep learning models in the clinical setting.

8. Acknowledgements

We would like to acknowledge the Stanford Program for Artificial Intelligence in Medicine and Imaging for clinical dataset infrastructure support (AIMI.stanford.edu).

References

- 2017. URL <http://www.boneandjointburden.org/2014-report>.
- AIMI. Artificial intelligence in medicine & imaging: Available labeled medical datasets. <https://aimi.stanford.edu/available-labeled-medical-datasets>. [Online; accessed 2-December-2017].
- Berlin, Leonard. Liability of interpreting too many radiographs. *American Journal of Roentgenology*, 175(1):17–22, 2000.
- Bhargavan, Mythreyi and Sunshine, Jonathan H. Utilization of radiology services in the united states: levels and trends in modalities, regions, and populations. *Radiology*, 234(3):824–832, 2005.
- Demner-Fushman, Dina, Kohli, Marc D, Rosenman, Marc B, Shooshan, Sonya E, Rodriguez, Laritza, Antani, Sameer, Thoma, George R, and McDonald, Clement J. Preparing a collection of radiology examinations for distribution and retrieval. *Journal of the American Medical Informatics Association*, 23(2):304–310, 2015.
- Deng, Jia, Dong, Wei, Socher, Richard, Li, Li-Jia, Li, Kai, and Fei-Fei, Li. Imagenet: A large-scale hierarchical image database. In *Computer Vision and Pattern Recognition, 2009. CVPR 2009. IEEE Conference on*, pp. 248–255. IEEE, 2009.
- Esteva, Andre, Kuprel, Brett, Novoa, Roberto A, Ko, Justin, Swetter, Susan M, Blau, Helen M, and Thrun, Sebastian. Dermatologist-level classification of skin cancer with deep neural networks. *Nature*, 542(7639):115–118, 2017.

Fitzgerald, Richard. Error in radiology. *Clinical radiology*, 56(12):938–946, 2001.

Gale, W., Oakden-Rayner, L., Carneiro, G., Bradley, A. P., and Palmer, L. J. Detecting hip fractures with radiologist-level performance using deep neural networks. *ArXiv e-prints*, November 2017.

Gertych, Arkadiusz, Zhang, Aifeng, Sayre, James, Pospiech-Kurkowska, Sylwia, and Huang, HK. Bone age assessment of children using a digital hand atlas. *Computerized Medical Imaging and Graphics*, 31(4):322–331, 2007.

Grewal, Monika, Srivastava, Muktabh Mayank, Kumar, Pulkit, and Varadarajan, Srikrishna. Radnet: Radiologist level accuracy using deep learning for hemorrhage detection in ct scans. *arXiv preprint arXiv:1710.04934*, 2017.

Gulshan, Varun, Peng, Lily, Coram, Marc, Stumpe, Martin C, Wu, Derek, Narayanaswamy, Arunachalam, Venugopalan, Subhashini, Widner, Kasumi, Madams, Tom, Cuadros, Jorge, et al. Development and validation of a deep learning algorithm for detection of diabetic retinopathy in retinal fundus photographs. *Jama*, 316(22):2402–2410, 2016.

Hannun, Awni, Case, Carl, Casper, Jared, Catanzaro, Bryan, Diamos, Greg, Elsen, Erich, Prenger, Ryan, Satheesh, Sanjeev, Sengupta, Shubho, Coates, Adam, et al. Deep speech: Scaling up end-to-end speech recognition. *arXiv preprint arXiv:1412.5567*, 2014.

Heath, Michael, Bowyer, Kevin, Kopans, Daniel, Moore, Richard, and Kegelmeyer, W Philip. The digital database for screening mammography. In *Proceedings of the 5th international workshop on digital mammography*, pp. 212–218. Medical Physics Publishing, 2000.

Huang, Gao, Liu, Zhuang, Weinberger, Kilian Q, and van der Maaten, Laurens. Densely connected convolutional networks. *arXiv preprint arXiv:1608.06993*, 2016.

Jaeger, Stefan, Candemir, Sema, Antani, Sameer, Wang, Yi-Xiang J, Lu, Pu-Xuan, and Thoma, George. Two public chest x-ray datasets for computer-aided screening of pulmonary diseases. *Quantitative imaging in medicine and surgery*, 4(6):475, 2014.

Kingma, Diederik and Ba, Jimmy. Adam: A method for stochastic optimization. *arXiv preprint arXiv:1412.6980*, 2014.

Krupinski, Elizabeth A, Berbaum, Kevin S, Caldwell, Robert T, Schartz, Kevin M, and Kim, John. Long radiology workdays reduce detection and accommodation accuracy. *Journal of the American College of Radiology*, 7(9):698–704, 2010.

Lu, Ying, Zhao, Shoujun, Chu, Philip W, and Arenson, Ronald L. An update survey of academic radiologists' clinical productivity. *Journal of the American College of Radiology*, 5(7):817–826, 2008.

Nakajima, Yasuo, Yamada, Kei, Imamura, Keiko, and Kobayashi, Kazuko. Radiologist supply and workload: international comparison. *Radiation medicine*, 26(8):455–465, 2008.

OAI. Osteoarthritis initiative: a multi-center observational study of men and women. <https://oai.epi-ucsf.org/datarelease/>. [Online; accessed 2-December-2017].

Rajpurkar, Pranav, Zhang, Jian, Lopyrev, Konstantin, and Liang, Percy. Squad: 100,000+ questions for machine comprehension of text. *arXiv preprint arXiv:1606.05250*, 2016.

Rajpurkar, Pranav, Hannun, Awni Y, Haghpanahi, Masoumeh, Bourn, Codie, and Ng, Andrew Y. Cardiologist-level arrhythmia detection with convolutional neural networks. *arXiv preprint arXiv:1707.01836*, 2017a.

Rajpurkar, Pranav, Irvin, Jeremy, Zhu, Kaylie, Yang, Brandon, Mehta, Hershel, Duan, Tony, Ding, Daisy, Bagul, Aarti, Langlotz, Curtis, Shpanskaya, Katie, et al. Chexnet: Radiologist-level pneumonia detection on chest x-rays with deep learning. *arXiv preprint arXiv:1711.05225*, 2017b.

Shiraishi, Junji, Katsuragawa, Shigehiko, Ikezoe, Junpei, Matsumoto, Tsuneo, Kobayashi, Takeshi, Komatsu, Ken-ichi, Matsui, Mitate, Fujita, Hiroshi, Kodera, Yoshie, and Doi, Kunio. Development of a digital image database for chest radiographs with and without a lung nodule: receiver operating characteristic analysis of radiologists' detection of pulmonary nodules. *American Journal of Roentgenology*, 174(1):71–74, 2000.

Wang, Xiaosong, Peng, Yifan, Lu, Le, Lu, Zhiyong, Bagheri, Mohammadhadi, and Summers, Ronald M. Chestx-ray8: Hospital-scale chest x-ray database and benchmarks on weakly-supervised classification and localization of common thorax diseases. *arXiv preprint arXiv:1705.02315*, 2017.

Woolf, Anthony D and Pfleger, Bruce. Burden of major musculoskeletal conditions. *Bulletin of the World Health Organization*, 81(9):646–656, 2003.

Zhou, Bolei, Khosla, Aditya, Lapedriza, Agata, Oliva, Aude, and Torralba, Antonio. Learning deep features for discriminative localization. In *Proceedings of the IEEE Conference on Computer Vision and Pattern Recognition*, pp. 2921–2929, 2016.